Featured in Physics

Bending Instability of Rod-Shaped Bacteria

Luyi Qiu, John W. Hutchinson, and Ariel Amir
John A. Paulson School of Engineering and Applied Sciences, Harvard University, Cambridge, Massachusetts 02138, USA

(Received 3 August 2021; accepted 20 December 2021; published 1 February 2022)

A thin-walled tube, e.g., a drinking straw, manifests an instability when bent by localizing the curvature change in a small region. This instability has been extensively studied since the seminal work of Brazier nearly a century ago. However, the scenario of pressurized tubes has received much less attention. Motivated by rod-shaped bacteria such as *E. coli*, whose cell walls are much thinner than their radius and are subject to a substantial internal pressure, we study, theoretically, how this instability is affected by this internal pressure. In the parameter range relevant to the bacteria, we find that the internal pressure significantly postpones the onset of the instability, while the bending stiffness of the cell wall has almost no influence. This study suggests a new method to infer turgor pressure in rod-shaped bacteria from bending experiments.

DOI: 10.1103/PhysRevLett.128.058101

Introduction.—As can be intuited from everyday experience, a thin-walled cylindrical tube such as a drinking straw subject to bending reaches a critical curvature at which instability occurs, localizing most of the curvature change into a narrow region [Figs. 1(a) and 1(b)]. This instability has been extensively studied since the seminal work of Brazier nearly a century ago [1]. Brazier calculated, approximately, the external torque needed to bend the tube to a given curvature of its long axis, and found that the dependence is nonmonotonic with a maximal value. Localization of the curvature change is expected at the curvature where the torque reaches a maximum. This instability is characterized by its dependence on the geometry rather than material nonlinearity. Another candidate for instability of a thin-walled tube is the wrinkling effect. When the lateral compressive stress reaches a critical value the system will develop periodic structures on the surface to minimize elastic energy [2,3]. Under increasing overall curvature, the wrinkles grow and trigger localization of the overall curvature. An extensive study of the competition between wrinkling and the Brazier instability for thicker metal shells which undergo plastic deformation prior to experiencing the bending instability has been given by Kyriakides and Corona in their book on buckling of undersea pipelines [4].

As the tube is bent, whenever the Brazier or the wrinkling instability is reached, the stress localizes, resulting in the characteristic kinks shown in Figs. 1(a) and 1(b). It is not apparent *a priori* which of the two instabilities will occur first and this will be addressed. Further, we shall show that the structural instability can be used to infer the mechanical properties of the system, e.g., turgor pressure, for rod-shaped bacteria.

Model.—Here, we consider a pressurized capped cylindrical tube of radius R, thickness t, and length $L \gg R$ with inner pressure larger than the external pressure by p. We bend the pressurized shell to a longitudinal curvature κ with no axial constraint. Away from the capped ends, each cross section behaves identically, and we take one cross section in the (x, y) plane as a representative in Fig. 1(d). The incremental material response measured from the cylindrical pressurized state is taken to be linear though the cylindrical swelling due to p may involve nonlinear elastic deformation, depending on the constitutive model.

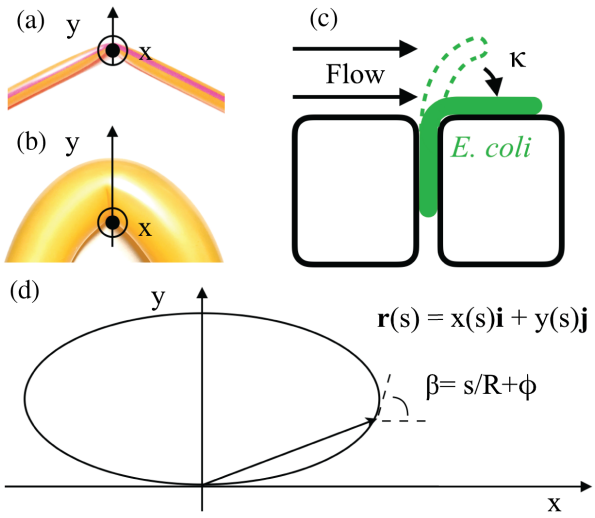

FIG. 1. Buckling of (a) a straw, (b) a birthday balloon, and (c) an *E. coli* cell in a mother machine. (d) Geometry notation. A deformed cross section is shown here. The points on the curve can be described by $\mathbf{r}(s) = x(s)\mathbf{i} + y(s)\mathbf{j}$ as a vector pointing from the coordinate origin to it. s is the distance measured along the curve. μ is corresponding dimensionless parameter $\mu = s/R$. β is the angle between the x axis and the vector tangent to the curve in the deformed configuration. $\phi(\mu)$ is the rotation angle, i.e., $\phi(\mu) = \beta - \mu$.

For rod-shaped bacteria such as *E. coli*, the elasticity of the cell wall is believed to be nonisotropic, presumably due to the preferential organization of the stiffer glycan strands in the circumferential direction and softer peptides along the longitudinal direction. Note also that the stresses on a pressurized cylinder are such that the circumferential stress is twice as large as the axial one, which for finite strains will also lead to nonisotropy. Therefore, we use the general orthotropic relation for stress and strain increments in the axial and circumferential directions (Supplemental Material, Sec. I [5]). For mathematical convenience and clarity, the deformation occurring during bending after p has been applied is assumed to be inextensional in the circumferential direction. This is similar to the hypothesis used by Euler in his elastica framework. The deformation occurring during bending is then fully characterized by the rotation function $\phi(\mu)$ defined in Fig. 1(d), the imposed curvature κ of the axial line element lying along $y = 0$, and the axial strain change $\Delta\varepsilon_0$ of that line element.

Prior to bending, the resultant membrane stresses are $N_\theta^0 = pR$ and $N_z^0 = pR/2$, and the bending moments in the tube wall are negligible. The change in the energy due to bending of the system under fixed p includes the sum of the changes in bending energy, stretching energy, and potential energy of pressure [17]. Under the circumferential inextensibility assumption, the circumferential membrane strain remains unchanged upon bending. The contribution to the bending energy in the wall of the tube associated with axial curvature $\Delta K_z \approx -\kappa$ is negligible compared to the axial stretching energy and is ignored. With $\Delta\Phi$ as the change in energy per unit length from the straight pressurized state, we have (Supplemental Material, Sec. I [5]):

$$\Delta\Phi = \int_0^{2\pi R} \left(N_z^0 \Delta\varepsilon_z + \frac{1}{2}\Delta N_z \Delta\varepsilon_z + \frac{1}{2}\Delta M_\theta \Delta K_\theta \right) ds - p\Delta V. \tag{1}$$

Here, $\Delta\varepsilon_z = \Delta\varepsilon_0 + \kappa y$ is the change of axial strain, $\Delta K_\theta = d\phi/ds$ is the circumferential curvature change, ΔV is volume change per unit length, $\Delta N_z = S_z \Delta\varepsilon_z$ is the increment of resultant membrane stresses, and $\Delta M_\theta = D_\theta \Delta K_\theta$ is the increment of shell wall bending moments. $S_\alpha = E_\alpha t/(1 - \nu_{\theta z}\nu_{z\theta})$ and $D_\alpha = S_\alpha t^2/12$ (α can be z or θ) are determined by material elastic properties. For imposed κ, $\Delta\Phi$ can be expressed in terms of $\Delta\varepsilon_0$ and $\phi(\mu)$ (Supplemental Material, Sec. I [5]):

$$\Delta\Phi = \frac{1}{2}\int_0^{2\pi} \left[\frac{D_\theta}{R^2}\left(\frac{d\phi}{d\mu}\right)^2 + S_z(\Delta\varepsilon_0 + \kappa y)^2 \right] R d\mu + p\pi R^2 \left[1 + \Delta\varepsilon_0 + \frac{\kappa}{2\pi}\int_0^{2\pi} y d\mu \right] - pR^2 \int_0^{2\pi} \frac{x}{R}(1 + \Delta\varepsilon_0 + \kappa y)\sin(\mu + \phi) d\mu. \tag{2}$$

For the convenience of calculation and presentation, it is useful to define and use nondimensional parameters. The equations can be rendered dimensionless in multiple ways. We can define a dimensionless geometry-material parameter in this system: $\alpha = \sqrt{(D_\theta/S_z R^2)} = \sqrt{(E_\theta/12E_z)}(t/R)$. Note that for thin tubes, $\alpha \ll 1$. For *E. coli* cells, $0.001 < \alpha < 0.01$ (Supplemental Material, Sec. II [5]). For thin shells, it is common to use the following dimensionless variables:

$$\bar{\Phi} = \frac{R}{D_\theta}\Delta\Phi, \quad \bar{p} = \frac{pR^3}{D_\theta}, \quad \bar{\kappa} = \frac{\kappa R}{\alpha}, \quad \bar{M} = \frac{M}{\alpha S_z R^2}, \tag{3}$$

in which M is the external torque needed to bend the tube. The "shell" normalization is employed under the tacit assumption that $\bar{p}$ is of order unity [18]. However, for *E. coli*, $\bar{p} = O(10^4)$ (Supplemental Material, Sec. II [5]). Consequently, in this pressure range it is more natural to use the following "balloon" normalization favoring the stretching stiffness:

$$\hat{\Phi} = \frac{\Delta\Phi}{S_z R}, \quad \hat{p} = \frac{pR}{S_z}, \quad \hat{\kappa} = \kappa R, \quad \hat{M} = \frac{M}{S_z R^2}. \tag{4}$$

Note that $\hat{p} = \alpha^2 \bar{p}$ such that for the *E. coli* cells $\hat{p}$ is of order unity (Supplemental Material, Sec. II [5]). In the results to follow we will illustrate both the shell and balloon normalizations. While the dimensionless quantities are different from one another, the form of the underlying governing equations is the same.

The state of the system for any imposed κ can be determined by minimizing $\Delta\Phi$ with respect to the rotation function $\phi(\mu)$ and $\Delta\varepsilon_0$. $\Delta\varepsilon_0$ can also be determined by a force-balance equation (Supplemental Material, Sec. III [5]). To further proceed, $\phi(\mu)$ is discretized using a Fourier series representation. Symmetry of the system about the y axis requires $\phi(\mu) = -\phi(2\pi - \mu)$, and the boundary condition: $x(2\pi) = x(0) = 0$ must be enforced. These lead to

$$\phi(\mu) = \sum_{n=1}^{N} a_n \sin(n\mu), \qquad 0 = \int_0^{2\pi} \cos[\mu + \phi(\mu)] d\mu. \tag{5}$$

For the special case of zero pressure, one can develop an approximate analytical solution for a_n by expanding the integrands of $x(\mu) = R\int_0^\mu \cos(\mu' + \phi) d\mu'$ and $y(\mu) = R\int_0^\mu \sin(\mu' + \phi) dq\mu'$ using Taylor expansions of ϕ (Supplemental Material, IV [5]). In the shell nondimensionalization,

$$a_n = -\frac{\bar{\kappa}^2}{4(n-1)^2 n^2} a_{n-2}, \qquad a_1 = 0, \qquad a_2 = -\frac{\bar{\kappa}^2}{8}. \tag{6}$$

The dominant coefficient a_2 is required to have a small absolute value in our solution. This solution agrees with Brazier's result for zero pressure.

For nonzero positive pressure, we use the ansatz $\phi(\mu) = a_2 \sin(2\mu)$ as an approximation whose accuracy will be

verified by numerical solutions shown later. Following the same Taylor expansion approximation, we obtain (Supplemental Material, Sec. IV [5]):

$$a_2 = -\frac{\bar{\kappa}^2}{8(1+\bar{p}/3)} = -\frac{\hat{\kappa}^2}{8(\alpha^2+\hat{p}/3)}. \tag{7}$$

This allows us to compute the overall torque-curvature relation and the dependence of the maximal torque on the pressure. To compute the torque-curvature relation we use $M = (\partial\Delta\Phi/\partial\kappa)$ which gives for the two normalizations (Supplemental Material, Sec. V [5]):

$$\bar{M} = \pi\left[\bar{\kappa} - \frac{\bar{\kappa}^3}{8(1+\bar{p}/3)}\right] \quad \text{or} \quad \hat{M} = \pi\left[\hat{\kappa} - \frac{\hat{\kappa}^3}{8(\alpha^2+\hat{p}/3)}\right]. \tag{8}$$

The critical curvature κ_B for the Brazier instability occurs at the maximum of external torque M:

$$\bar{\kappa}_B = \sqrt{\frac{8}{3}+\frac{8}{9}\bar{p}} \quad \text{or} \quad \hat{\kappa}_B = \sqrt{\frac{8}{3}\alpha^2+\frac{8}{9}\hat{p}}. \tag{9}$$

Equation (9) reveals that the pressure can greatly postpone the onset of the Brazier instability. Interestingly, a_2 at the maximal torque is a constant $-1/3$ independent of material properties and the inner pressure. In other words, the shape of the cross section at the critical state is always the same for the Brazier instability. At the maximal torque, the tube cross section is squeezed in the y direction by about 22% and its second moment is reduced by about 40%.

An accurate estimate of the onset of the wrinkling instability is obtained by making use of the formula for the axisymmetric buckling of a pressurized circular cylindrical shell of radius ρ and thickness t subject to a compressive axial stress σ. For a shell with the present incremental orthotropic properties, the critical compressive stress σ_c and the associated axial wavelength l of the sinusoidal wrinkling mode are

$$\sigma_c t = \frac{2}{\rho}\sqrt{D_z S_\theta}, \qquad l = 2\pi\left(\frac{D_z}{S_\theta}\rho^2\right)^{1/4}. \tag{10}$$

These formulas apply approximately to the wrinkling instability of the tube under bending if one identifies the critical stress with the maximal compressive stress in the ovalized tube, and ρ is the circumferential radius of curvature at the position of maximal compression. The validity of the approximation stems from the fact that the wrinkling mode has a wavelength proportional to $\sqrt{\rho t}$ which is short compared to the radius of the tube. Detailed calculations in the shell buckling literature [3] have shown that the critical stress given by Eq. (10) underestimates the local compressive stress at the onset of wrinkling in a thin elastic shell under bending by only a few percent. The thinner the shell, the more accurate the approximation. In summary, the onset of the wrinkling instability is attained when the curvature κ is sufficiently large so that $N_z^0 + \Delta N_z = -\sigma_c t$ according to the critical stress in Eq. (10). Employing the balloon normalization [Eq. (4)] with the expressions for a_2 [Eq. (7)] and $\Delta\varepsilon_0$, one can obtain the following dimensionless equation for the overall curvature $\hat{\kappa}_w$ at the onset of wrinkling (Supplemental Material, Sec. VI [5]):

$$8\left(\alpha^2+\frac{\hat{p}}{3}\right)\left(\frac{\hat{p}}{2}+2\alpha-\hat{\kappa}_w\right)+\left(\frac{2\hat{\kappa}_w}{3}-4\alpha\right)\hat{\kappa}_w^2 = 0, \tag{11}$$

with the associated torque given by Eq. (8). Two special limits are worth noting. If $\hat{p}=0$, Eq. (11) becomes $\bar{\kappa}_w^3 - 6\bar{\kappa}_w^2 - 12\bar{\kappa}_w + 24 = 0$, with the smallest positive solution $\bar{\kappa}_w = 1.320$. Thus, for the unpressurized tube, wrinkling occurs before the Brazier instability $\bar{\kappa}_B = \sqrt{8/3} \approx 1.633$. The other limit applies when the pressure is in the "balloon range" and the tube is thin ($\alpha \ll \hat{p}$) such that α is negligible in Eq. (11), leading to $\hat{\kappa}_w^3 - 4\hat{p}\hat{\kappa}_w + 2\hat{p}^2 = 0$. We therefore obtain $\hat{\kappa}_w = (\hat{p}/2) + O(\hat{p}^2)$.

Numerical results.—The torque-curvature relation [Eq. (8)] for the two normalizations is plotted in Fig. 2 for various relevant dimensionless pressures where they can be compared with numerical results based on minimization of the energy functional $\Delta\Phi$ in Eq. (2) (Supplemental Material, Sec. VII [5]). Included in Fig. 2 on each of the torque-curvature curves are solid dots marking the onset of the wrinkling instability computed numerically. They agree well with the crosses, which are the wrinkling curvatures predicted [Eq. (11)]. Over the entire range of pressures, in shell normalization or balloon normalization, wrinkling precedes attainment of the maximal moment, increasingly so as the pressure increases. Note that in the balloon regime wrinkling occurs on the initial linear segment of the torque-curvature curve for which $\hat{M} \approx \pi\hat{\kappa}$. The validity of the incremental formulation is limited to relatively small incremental strains, not greater than 0.2. The maximal axial strains due to bending are of the order of κR. Note that for $\hat{p} = 0.4$ the critical wrinkling curvature is $\kappa_w R \approx 0.2$. Thus, the wrinkling predictions are expected to be valid in the range $\hat{p} < 0.4$.

A method to measure turgor pressure.—Our results can be utilized to provide a novel protocol for measuring turgor pressure in bacteria [Fig. 1(c)] (see Supplemental Material, Sec IX [5]), a task which has proved challenging over decades [6]. Previous works have shown that one may grow filamentous bacteria with large length to diameter ratios and bend them either with optical tweezers [7] or with force generated by viscous drag due to fluid flow [8]. According to our results and for the relevant parameter range for *E. coli*, as long as the wrinkling instability is not reached cell bending will be approximately linear in the torque and independent of pressure, as validated experimentally [8]. This torque-curvature relationship also provides a way to

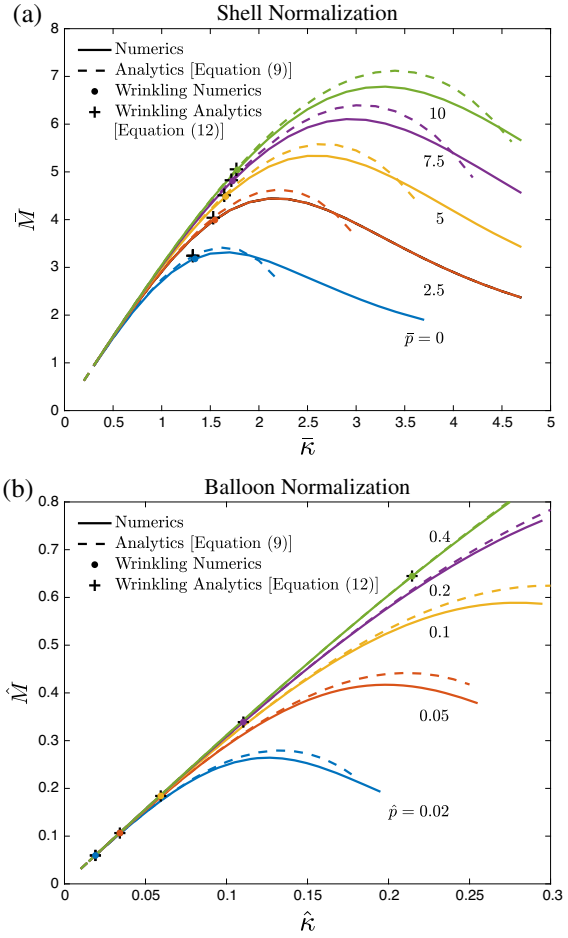

FIG. 2. Comparison of analytical and numerical results for torque-curvature relation and onset of wrinkling for typical elastic properties of *E. coli* (Supplemental Material, Sec. II, $\alpha \approx 0.005$ [5]). (a) Shell normalization for low pressures. (b) Balloon normalization for high pressures. The dashed lines are given by the formulas in Eq. (8), while the solid lines are based on the numerical minimization of $\Delta\Phi$ (Supplemental Material, Sec. VII [5]). The black cross is the onset of wrinkling predicted by Eq. (11). The color dots indicate the onset of wrinkling computed numerically. The critical curvatures for systems with different α are shown in Supplemental Material, Sec. VIII [5].

infer S_z as we discuss in detail in Supplemental Material, Sec. I [5]. Note, however, that here the incremental modulus S_z can depend on p. If the osmolarity of the media surrounding the cell is suddenly increased (by, e.g., adding sugar) the turgor pressure drops abruptly [19], while the torque on the cell remains unperturbed. If the new turgor pressure is sufficiently low such that the wrinkling instability is reached—as quantified by Eq. (11)—the cell would immediately buckle. Therefore, by repeating this experiment for varying degrees of the hyperosmotic shock, the turgor pressure can be accurately measured. In fact, preliminary results using this protocol have shown it is feasible to achieve cell buckling upon osmotic shock for wild-type filamentous *E. coli* [20]. *A priori* one might have envisioned that an alternative way to infer turgor pressure is from the M-κ curve as indicated by Eq. (8). However, for the parameters of *E. coli*, the M-κ curve shows barely any nonlinearity before the instability point, as shown in Fig. 2.

Discussion.—In this work we revisited the long-standing problem of the Brazier effect, albeit for the understudied yet highly relevant scenario of a pressurized tube. While in structural mechanics applications the relevant pressure regimes are typically assumed to be associated with shells, where the pressure is sufficiently small in comparison with the bending rigidity, microbes such as bacteria are found to be in a qualitatively different "balloon" regime with tremendous pressures outside the scope of previous theoretical work. By treating the problem using an elastica framework we were able to obtain analytical formulas for the two potential instabilities that may arise when bending such highly pressurized tubes: one associated with a maximum in the torque-curvature relation, and the other associated with the onset of wrinkling at a critical compressive stress. We corroborated our results numerically, finding good agreement between the approximate theory (assuming a particular mode of deformation dominates) and the precise numerics.

Within our theoretical approach, we found that the torque-curvature relations are well approximated by a linear dependence with a pressure-independent slope, and a cubic curvature contribution that strongly depends on the pressure as $[1/(1+pR^3/3D_\theta)]$. Thus, for high pressures this factor scales inversely with the pressure. This flattening of the torque-curvature relation can be associated to the ovalization of the cross sections, that become approximately elliptical as the tube is bent. The high pressure resists this effect and tends to maintain a circular cross section. Indeed, the dominant mode of deformation of the cross section scales as $\sin(2\mu)$, and its magnitude follows the same functional dependence on p as the nonlinear term in the torque-curvature relation. Interestingly, Calladine solved the related problem of deformation of a pressurized *straight* shell subject to periodic loading, and found that the effect of pressure is to repress the cross-section deformation via precisely the same functional form described above [18]. For a particular model of elasticity known as the Varga model, the Brazier effect was numerically studied under the assumption that bending rigidity is negligible [21]. Our analytical results suggest that bending rigidity is indeed unimportant in the "balloon regime" and provides a quantitative criterion for it.

Another point of biological relevance regards the *existence* of the turgor pressure in wild-type *E. coli*. We note that using Eq. (11), in the absence of turgor pressure the cells would buckle at the remarkably small curvature of $0.6\%(1/R)$; in other words, the cell wall would collapse upon any minor mechanical perturbation. The turgor pressure therefore plays an important role in stabilizing the shell, though this point has been largely overlooked in

the biological literature. For the *E. coli* parameters, the critical curvature for the wrinkling instability is predicted to be of the order of the inverse cell radius, allowing the cell to undergo severe mechanical deformations. This is consistent with the remarkable flexibility of growing cells to adapt to narrow microfluidic constrictions [22].

In summary, we have provided here an analysis of the Brazier instability in thin, pressurized tubes, and fully characterized the dramatic role of pressure in suppressing the instability. This can be naturally used as a tool for measuring turgor pressure in bacteria, as well as other rod-shaped cell-walled organisms including plants.

In particular, the alga *Chara corallina* falls well within the regime we study here, despite having tremendously different length scales involved (see Supplemental Material, Sec. II [5]). Our results pave the way to future studies on pressurized shells. In particular, while here the analysis is performed at the level of linear incremental constitutive laws (though geometrical nonlinearities are fully accounted for), it would be interesting to see how the results would carry over to the case of neo-Hookean elastic models, or more elaborate models of bacterial cell walls. Our assumption of cross section inextensionality while bending the pressurized cylinder has enabled us to obtain analytical, closed-form solutions for the instability. This assumption has been used and verified in many relevant mechanical problems [23]. Nonetheless, it would be interesting to explore the accuracy of this assumption in future work. Furthermore, it would be useful to find how sensitive the onset of the instability is to imperfections, as has been studied in the context of other elastic instabilities of pressurized shells, albeit with external pressure larger than the internal one, leading to implosions [28,29]. Finally, it would be interesting to explore—analytically, numerically and experimentally—the development of the onset of wrinkling into an instability, as was studied in other systems in previous works [30,31].

We thank Felix Wong, Efi Efrati, and Hillel Aharony for insightful discussions. A. A. acknowledges funding from the Volkswagen Foundation, NSF CAREER Grant No. 1752024, and MRSEC Grants No. DMR-1420570 and No. DMR-2011754.

[1] L. G. Brazier and R. V. Southwell, Proc. R. Soc. **116**, 104 (1927).
[2] J. W. Hutchinson, Int. J. Solids Struct. **3**, 97 (1967).
[3] P. Seide and V. I. Weingarten, J. Appl. Mech. **28**, 112 (1961).
[4] S. Kyriakides and E. Corona, *Mechanics of Offshore Pipelines* (Elsevier, New York, 2007), Vol. 1.
[5] See Supplemental Material at http://link.aps.org/supplemental/10.1103/PhysRevLett.128.058101 for typical elastic properties of model organisms, supplementary derivations, numerical verification, and a detail discussion on the experimental method to measure turgor pressure, which includes Refs. [6–16].
[6] Y. Deng, M. Sun, and J. W. Shaevitz, Phys. Rev. Lett. **107**, 158101 (2011).
[7] S. Wang, H. Arellano-Santoyo, P. A. Combs, and J. W. Shaevitz, Proc. Natl. Acad. Sci. U.S.A. **107**, 9182 (2010).
[8] A. Amir, F. Babaeipour, D. B. McIntosh, D. R. Nelson, and S. Jun, Proc. Natl. Acad. Sci. U.S.A. **111**, 5778 (2014).
[9] X. Yao, M. Jericho, D. Pink, and T. Beveridge, J. Bacteriol. **181**, 6865 (1999).
[10] L. Gan, S. Chen, and G. J. Jensen, Proc. Natl. Acad. Sci. U.S.A. **105**, 18953 (2008).
[11] A. Koch, Res. Microbiol. **141**, 119 (1990).
[12] D. S. Cayley, H. J. Guttman, and M. T. Record, Biophys. J. **78**, 1748 (2000).
[13] G. Schubert, J. Fluid Mech. **27**, 647 (1967).
[14] J. S. Boyer, Frontiers of plant science **7**, 866 (2016).
[15] G. A. Toole, P. A. Gunning, M. L. Parker, A. C. Smith, and K. W. Waldron, Planta **212**, 606 (2001).
[16] R. E. Goldstein and J.-W. van de Meent, Interface Focus **5**, 20150030 (2015).
[17] L. D. Landau and E. M. Lifshitz, *Theory of Elasticity* (Elsevier, New York, 1986).
[18] C. R. Calladine, *Theory of Shell Structures* (Cambridge University Press, Cambridge, England, 1983).
[19] E. Rojas, J. A. Theriot, and K. C. Huang, Proc. Natl. Acad. Sci. U.S.A. **111**, 7807 (2014).
[20] Felix Wong and Sean Wilson (private communications).
[21] E. M. Haseganu and D. J. Steigmann, Int. J. Solids Struct. **31**, 27 (1994).
[22] F. Wong, L. D. Renner, G. Özbaykal, J. Paulose, D. B. Weibel, S. Van Teeffelen, and A. Amir, Nat. Rev. Microbiol. **2**, 17115 (2017).
[23] An example of the usage of this assumption in a classic problem is Euler's work on the buckling of a column under axial compression [24], where it leads to accurate results both for buckling and for the postbuckling behavior [25]. Carrier used this assumption to produce analytical solutions for the buckling of an elastic circumferential ring, accurate both for the initial buckling and in the advanced postbuckling range [26]. Brazier also assumed an inextensible cross section for calculating the deformation of an unpressurized, bent tube. The obtained M-κ (torque-curvature) curves have been tested and verified in experiments [27].
[24] L. Euler, *Methodus Inveniendi Lineas Curvas Maximi Minimive Proprietate Gaudentes* (Apud Marcum-Michaelem Bousquet, 1744).
[25] G. Domokos, P. Holmes, and B. Royce, in *Mechanics: From Theory to Computation* (Springer, New York, 2000), pp. 413–446.
[26] G. Carrier, J. Math. Phys. (N.Y.) **26**, 94 (1947).
[27] B. Reddy, Int. J. Solids Struct. **15**, 669 (1979).
[28] E. Virot, T. Kreilos, T. M. Schneider, and S. M. Rubinstein, Phys. Rev. Lett. **119**, 224101 (2017).
[29] J. Paulose and D. R. Nelson, Soft Matter **9**, 8227 (2013).
[30] H. Diamant and T. A. Witten, Phys. Rev. Lett. **107**, 164302 (2011).
[31] B. Davidovitch, R. D. Schroll, and E. Cerda, Phys. Rev. E **85**, 066115 (2012).